Central Catadioptric Line Detection

Pascal Vasseur and El Mustapha Mouaddib
C.R.E.A. (Centre de Robotique d'Electrotechnique et d'Automatique) EA3299
University of Picardie Jules Verne (U.P.J.V.)
7, rue du Moulin Neuf - 80 000 Amiens - France
E-mail:Pascal.Vasseur@sc.u-picardie.fr

Abstract

Central catadioptric sensors enable to acquire panoramic images on a 360 degree field of view while preserving a single viewpoint. These advantages account for the growing use of these sensors in applications such as surveillance, navigation or modelling. However, the deformations of the image do not allow to apply classical perspective image algorithms or operators. Typically, straight line detection in perspective image becomes a delicate and complex conic detection problem in central catadioptric image. Previous methods proposed in the literature were essentially motivated by particular cases such as horizontal line detection or paracatadioptric line detection. In this paper, we propose an algorithm which consists in performing the detection in the space of the equivalent sphere which is the unified domain of central catadioptric sensors. On this sphere, real lines are projected into great circles that we detect thanks to the Hough transform. We also propose to apply this unifying model in order to perform the calibration of the intrinsic parameters required for the projection on the sphere. We show results on synthetic and real catadioptric images (parabolic, hyperbolic) to demonstrate the relevance of the detection on the sphere.

1 Introduction

Omnidirectional sensors capture a very large field of view which provide significant advantages in comparison with classical cameras. Thus, applications such as surveillance, model construction, mobile robot localization and navigation increasingly integrate these sensors. In order to obtain a panoramic vision, different systems have been proposed such as a rotating camera, a camera network, a fish eye lens and the combination of a convex mirror with a conventional camera [5]. This last category named catadioptric sensors has received a lot of attention in the last ten years [15] [1] [12] [13].
Catadioptric sensors can be divided into two classes according to the constraint of the viewpoint [1]. We can differenciate respectively the central catadioptric sensors with a single viewpoint and the non-central catadioptric sensors which do not have a single viewpoint. This characteristic is very important because it permits the reconstruction of geometrically correct perspective images from the catadioptric images [2] and [1].

In this paper, we are particularly interested in the detection of central catadioptric lines which are very useful for applications such as tracking, localization or 3D reconstruction.

BMVC 2004 doi:10.5244/C.18.8

Line detection is a very well known problem in perspective images and numerous methods have been proposed to solve it [6] [10] [8]. However, for central catadioptric images, the problem becomes more complex and delicate to solve. Indeed, as demonstrated in [4] [9] [17], the image of any real straight line in 3D space is a conic in the catadioptric plane. In this case, it is necessary to estimate, for each conic, five parameters with methods such as those presented in [18]. However, these methods are generally computationally expensive and do not permit to obtain efficient results for real catadioptric images in which only small portions of these conics are visible.
In the following parts of this paper, we present our motivations and contributions in Section 2 followed by the model of a central catadioptric projection and the projection of a real line in Section 3. The detection algorithm is described in Section 4. Section 5 is dedicated to the experimental results with a brief discussion. Finally, we conclude in Section 6 with some perspectives.

2 Motivations and Contributions

Line detection is a very important problem in catadioptric imagery since it allows to perform higher level treatments such as localization [16] or 3D reconstruction [14] [11]. In [11], Fiala and Basu propose an algorithm based on an adaptation of the Hough transform which allows to detect horizontal real lines in the case of a spherical image (no single viewpoint). Every horizontal line is characterized by a fall-line corresponding to the line passing through the intersection of the vertical axis (optical axis of the camera) with the plane which contains the horizontal line and provides the minimum angle with the vertical axis. Thus, for each point in the image, a set of fall-lines is defined. The panoramic Hough space is then bi-dimensional. A Look-up table is finally used in order to speed up the treatment and a panoramic stereo reconstruction is proposed as an application. In [4], Barreto and Araujo propose a method which allows the detection of any real straight lines in paracatadioptric images (parabolic mirror with orthographic camera). The authors propose to perform the detection directly in the image and to compare different methods of parameter estimation [18]. They also present an algorithm which ensures that detected conics effectively correspond to real 3D lines. In this way, they integrate a new constraint based on the circular and conjugate points of the conic. The estimation of the parameters is then finally solved by a spectral analysis of a matrix which minimizes the algebraic distance between the data points and the conic curve. This approach provides an efficient and accurate algorithm. However, only paracatadioptric images can be treated with this approach and the problem of conic estimation may become a problem of circle detection, since the paracatadioptric images of real lines are arcs of circles if the camera aspect ratio is unitary and there is no skew [9]. Moreover, the results on real images are obtained after a manual selection of two points for each conic.

We propose to work on the sphere associated to the sensor and not directly on the image. As demonstrated in [4] and [9], a 3D straight line is first projected into a great circle on the equivalent sphere. This great circle has the same center and the same radius as the sphere. We then propose to realize the detection of these great circles, and consequently of the corresponding lines directly in the domain of the sphere with a simple adaptation of the Hough transform. However, the transformation on the sphere requires

to know the intrinsic parameters of the sensor. This is why some authors argue that the adaptation of treatments for central catadioptric images is not necessary since it is always possible to compute the equivalent perspective images [11]. However, line detection requires a preprocessing of the perspective image in order to extract the edges. To apply classical perspective operators, it is necessary to correct the discrete deformations by an intensity interpolation and a resampling of the perspective image. However, this approach is computationally expensive and the interpolation may yield false information. For these reasons, we adopt the point of view presented in [7] which consists in adapting treatments to the catadioptric images. The authors propose in their paper some operators adapted to the central catadioptric images by performing the treatments in the domain of the sphere. In this way, the contribution is to propose the possibility to perform a sequence of treatments (preprocessing, feature detection and high-level treatments such as localization, reconstruction, ...) in a unified domain (the equivalent sphere). From these points of view, it appears interesting to perform the detection on the sphere. Of course, it is necessary to calibrate and we also propose to directly estimate the intrinsic parameters with a single algorithm for the whole set of central mirrors, which is also an advantage.

3 Central Catadioptric Projection Model and Calibration

In this part, we provide the central catadioptric projection model that we adopt in order to explain and discuss our choices. For interested readers, we suggest the following references for further details and explanations [3] [9].

A catadioptric vision system is the association of a reflected mirror with a camera. Whatever the shape of the mirror surface, it is desirable that the axis of revolution of the mirror is in line with the optical axis of the camera. In [3], a succinct review of the different sensors with the equations of the different shapes of mirrors are presented. Schematically, the projection of a 3D real point is performed in two steps. The first one deals with the projection of 3D point P_r into point P_m on the surface of the mirror. The second step is the reflection of P_m in a point P_i in the image. Among the developed models which provide the mapping function between point P_r and point P_i, we choose more particularly the model based on the equivalent sphere [9]. In this model, the mapping function is equivalent to a projection from point P_r onto the sphere, followed by a projection from a point on the sphere axis to the image plane. The center of the sphere is equal to the mirror focus and its radius is function of the latus rectum of the mirror (also equal to $4h$). The position of the center of projection in the second projection depends on the shape and the dimensions of the mirror (Figure 1).

In figure 1, $4h$ is equal to the latus rectum of the mirror and x_s, y_s and z_s are the coordinates of 3D point $P_r = (x_r, y_r, z_r)$ projected on the sphere and equal to :

$$\begin{aligned} x_s &= \gamma x_r \\ y_s &= \gamma y_r \\ z_s &= \gamma z_r \end{aligned} \tag{1}$$

The equation of the sphere is $x_s^2 + y_s^2 + z_s^2 = R^2$ and then gives :

$$\gamma = \frac{R}{\sqrt{x_r^2 + y_r^2 + z_r^2}} \tag{2}$$

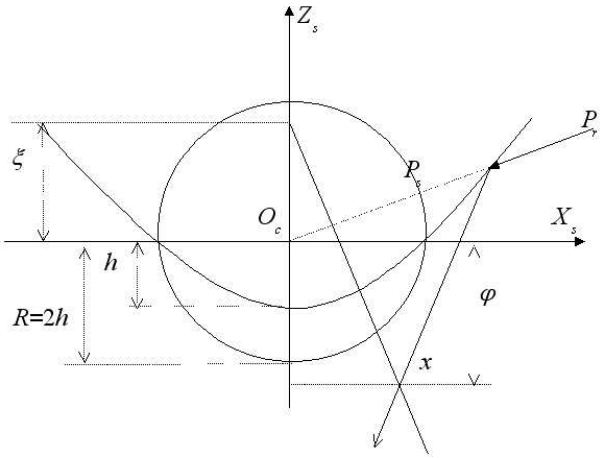

Figure 1: Illustration of the theorem of equivalence for the paracatadioptric case.

The coordinates of point P_i on the image plane are then obtained from a perspective projection of P_s and the parameters of the mirror (ξ,φ) :

$$\begin{array}{l} \frac{x_s}{\xi - z_s} = \frac{x}{\xi + \varphi} \\ \frac{y_s}{\xi - z_s} = \frac{y}{\xi + \varphi} \\ z = -\varphi \end{array} \tag{3}$$

$$\begin{array}{l} x = \frac{(\xi+\varphi)Rx_r}{\xi\sqrt{x_r^2+y_r^2+z_r^2}-Rz_r} \\ y = \frac{(\xi+\varphi)Ry_r}{\xi\sqrt{x_r^2+y_r^2+z_r^2}-Rz_r} \\ z = -\varphi \end{array} \tag{4}$$

In the image frame, we finally obtain :

$$\begin{pmatrix} u \\ v \end{pmatrix} = \begin{pmatrix} \alpha_u & 0 & u_0 \\ 0 & \alpha_v & v_0 \end{pmatrix} \begin{pmatrix} x \\ y \\ 1 \end{pmatrix} \tag{5}$$

In order to perform the calibration with the previously described model, we place the catadioptric system in an opened cube with a grid of points on each side (figure 2). In this way, the points of the pattern are distributed over the whole catadioptric image. The pattern contains 112 points and we calculate six extrinsic parameters (3 rotations and 3 translations) as well as the intrinsic parameters of the camera $(\xi, \varphi, \alpha_u, \alpha_v, u_0, v_0)$. The estimation is performed by the minimization of the quadratic error between the selected points and those computed by the model.

From the estimated parameters and the theorem of equivalence, it is easy to obtain the coordinates of the points on the sphere from the coordinates in the image by inverting equations 3 and by using the equation of the sphere.

Figure 2: Calibration system.

4 Central Catadioptric Lines Detection Algorithm

From the model previously developed, it is obvious that the projection of a 3D line on the sphere is a great circle and the projection of this great circle on the catadioptric plane is a conic in the general case [4] [9]. Detecting the projection of a real line in the catadioptric image plane then consists in estimating the parameters of the conic. As mentioned in [18], even if this problem is one of the simplest problems in computer vision, it is a relatively difficult problem because of its nonlinear nature. Moreover, an automatic detection requires the testing of the set of possible conics for each treated pixel and then increases the complexity of the estimation. In this paper, we are interested by the detection of real lines captured by any central catadioptric sensor. Figure 3 shows the image of a 3D line with different positions and orientations captured by a hyperbolic sensor. In fact, a weak displacement of the line can radically modify the nature of the conic. Our proposition is then to perform the detection in the domain of the sphere where any 3D line captured by any central catadioptric sensor corresponds to a great circle. This unified proposition brings several advantages. First, since the great circles have the same center and the same radius as the sphere, the space of research is reduced to a unique degree of freedom for each treated pixel (figure 4). Second, the research in the domain of the sphere is a natural following of the low-level operators proposed in [9] and permits to improve the computation time. Finally in [4], Barretto and Araujo impose constraints which ensure that each detected conic is the image of a real line. In our approach, a great circle is necessarily the image of a curve included in the plane which passes through the center of the sphere and which contains the great circle. In real applications, this curve is practically always a straight line.

A real 3D line becomes a great circle on the sphere which can be represented by its normal characterized by the elevation θ and the azimuth ρ (figure 4). The adapted Hough space is then based on these angles. In this way, for each treated pixel, the set of great circles which passes through this pixel on the sphere can be represented by the lines which pass through the center of the sphere and are perpendicular to the line represented by the center of the sphere and the treated pixel. In order to illustrate the duality between the space of the image and the Hough space, figure 5 presents both spaces with their respective correspondences. A point in the Hough space represents a conic in the image (respectively a great circle on the sphere), and a point in the image gives a curve in the Hough space. The computation of the normal for each great circle is performed from the scalar product between the line passing through the center of the sphere and point P_s on the sphere, and the normal passing through the center of the sphere and point P_n placed on the sphere. We finally obtain the expression of elevation θ in function of azimuth ρ and the coordinates of pixel P_s on the sphere (x_s, y_s, z_s) (equation 6). The algorithm then

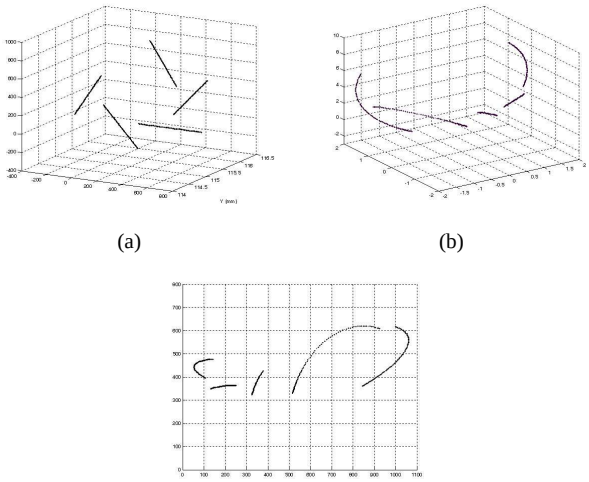

(a) (b)

(c)

Figure 3: Examples of 3D line projections on a hyperbolic mirror: (a) 3D lines in space with different positions and orientations, (b) Projection of the lines on the hyperbolic mirror, (c) Projection on the image plane.

simply consists in sampling the interval of definition of ρ and in computing the correspondant values of θ in order to increment the accumulator.

$$\theta = atan\left(-\frac{x_s cos(\rho) + y_s sin(\rho)}{z_s}\right) \tag{6}$$

We can remark that the complexity of this algorithm is very low and only depends on the number of pixels and the number of values for angle ρ. As in [11], a look-up table could be used in order to avoid the computation of θ. Since in the Hough transform, the detection of the peaks in the accumulator is a delicate operation, we also propose to perform the algorithm independently for each connected edge group. This improvement enables to manage a low number of peaks at each iteration and to obtain the endpoints of each detected segment.

5 Experimental Results

We first present the calibration results computed for both parabolic and hyperbolic mirrors (Table1). Each calibration has been realized from a dozen of images of the pattern and we obtain for both mirrors a mean error equal to 1.2 pixel and a standard deviation equal to 0.5 pixel. The NetVision objective (paracatadioptric sensor) is made of a convex parabolic mirror and a concave spherical mirror which is used as a telecentric lens for an orthographic projection.

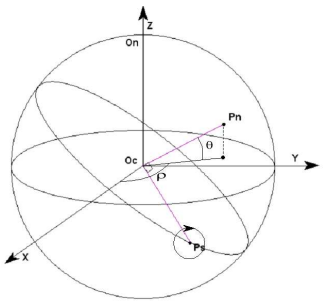

Figure 4: Great circles computation for a point on the sphere.

	Pixels/mm		Optical center		Mirror			Error	
	α_u	α_v	u_0	v_0	ξ	φ	R	$\bar{m}$	σ
Parabolic	-120.59	120.09	387.48	274.95	1.14	1.40	1	1.28	0.52
Hyperbolic	-144.81	145.08	421.20	278.77	-0.91	-0.48	1	1	0.5

Table 1: Results of calibration for parabolic and hyperbolic mirrors.

In figure 6(a), we have simulated an environment with only horizontal and vertical real lines projected on a paracatadioptric image. In this case, all the lines are perfectly detected (figure 6(b)). We use this synthetic environment in order to test the sensitivity of the detection according to the calibration parameters. We have performed some tests with modified intrinsic parameters useful for the projection on the sphere. We first modified ξ and φ with a tolerance of 0.2 for 100 images. The lines have always been detected with an error equal to 0.1 radian for the azimuth and the elevation of the horizontal lines and 0 radian for the azimuth and the elevation of the vertical lines. We have made 100 other tests by adding a tolerance of five percent for u_0 and v_0. In 86 cases all the lines were detected. The errors for the azimuth and the elevation are respectively equal to 0.02 and 0.38 radians for the horizontal lines and 0.12 and 0 for the vertical lines. The center of the image then appears more important than the mirror parameters. However, in catadioptric sensor calibration, the estimation of u_0 and v_0 is particularly accurate and we have always found the same coordinates whatever the calibration method for both mirrors. The images are all of size 768 by 576 and in our current implementation, the complete treatment takes about three seconds with Matlab 5.3.

Finally, we propose some results on real parabolic (figure 6(c)(d)) and hyperbolic (figure 6(e)) images. We found some over-detection due to the Hough accumulator but an adaptation of the peak detection could surely improve the result. For the first real catadioptric image (figure 6(c)), we obtain 30 detected lines and about 100 for images on figures 6(d) and (e). We have only represented some detected lines for the real images for convenience of visualization purpose.

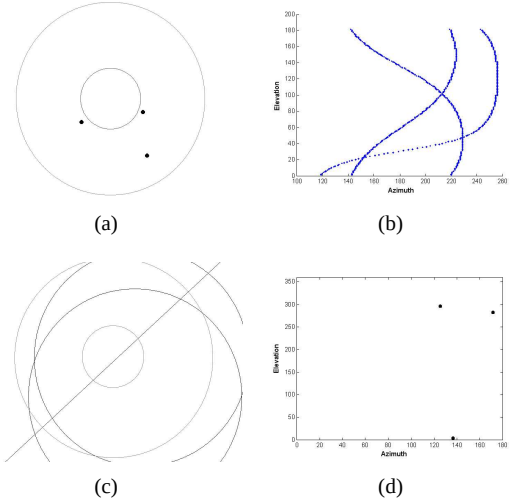

(a) (b)

(c) (d)

Figure 5: Duality of image space and Hough space - (a) Image with three points, (b) Corresponding Hough space with three curves, (c) Three central catadioptric lines detected in the image, (d) Corresponding three points in Hough space.

6 Conclusion

In this paper, we propose an original algorithm for central catadioptric lines detection. Contrary to previous methods, our approach consists in performing the detection in the domain of the sphere where the real lines are transformed in great circles. These circles have the same center and the same radius as the sphere. These characteristics allow to fix constraints on the space search and then to obtain efficient results with a simple adaptation of the Hough transform. The proposed method is also a contribution in the sense that it allows to detect any real 3D line in the image captured by any central catadioptric sensor. We then also propose an efficient method to calibrate parameters needed for the equivalent sphere model and for intrinsic parameters of the camera. So, our method for lines detection has several advantages such as simplicity, efficiency and real time. All these advantages are important in the context of mobile robot perception, where we often need to calibrate the sensor and to extract features in real time. As future works, the central line detection will be integrated in a system of 3D environment reconstruction for a mobile robot.

References

[1] S. Baker and S.K. Nayar. A theory of catadioptric image formation. In *International Conference Computer Vision 98, India*, pages 35–42, 1998.

[2] S. Baker and S.K. Nayar. A theory of single-viewpoint catadioptric image formation. *International Journal on Computer Vision, Kluwer Academic*, 35(2):175–196,

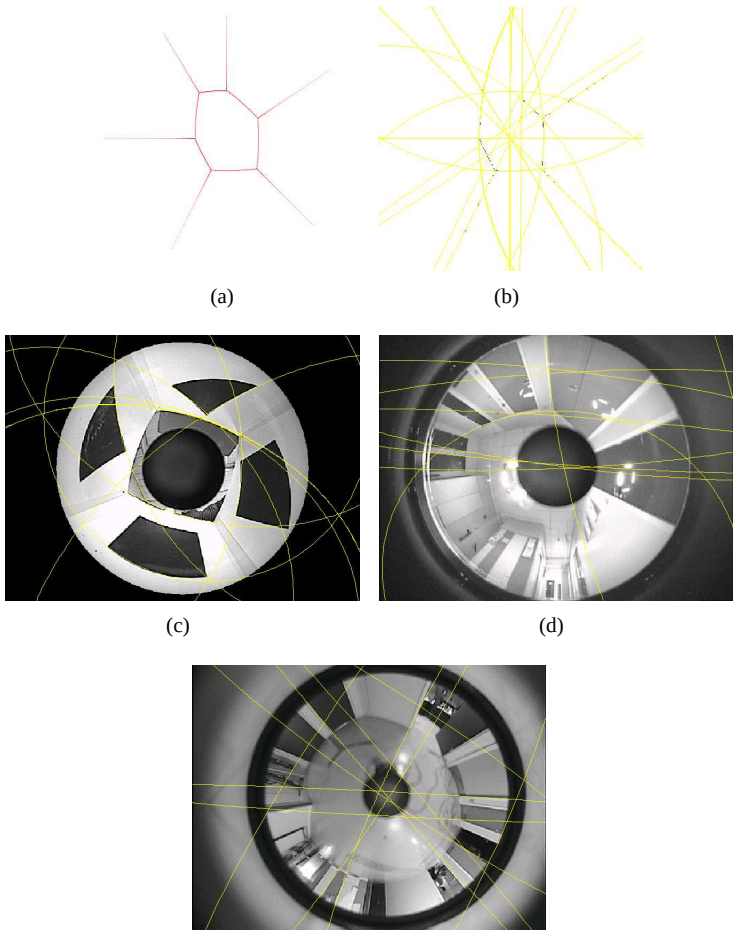

Figure 6: Experimental results (a) Paracatadioptric synthetic image, (b) The whole set of detected lines, (c) and (d) Representation of ten and five lines detected in real paracatadioptric images, (e) Representation of five detected lines in a real hypercatadioptric image - The number of lines is limited for convenience of visualization purpose.

November 1999.

[3] J.P. Barreto and H. Araujo. Issues on the geometry of central catadioptric image formation. In *International Conference Computer Vision 01, Hawaii*, pages II:422–427, 2001.

[4] J.P. Barreto and H. Araujo. Direct least square fitting of paracatadioptric line images. In *Omnivis 2003: Workshop on Omnidirectional Vision and Camera Networks, held with CVPR*, 2003.

[5] R. Benosman and S.B. Kang. *Panoramic Vision: Sensors, Theory, Applications*. Springer, 2001.

[6] J.B. Burns, A.R. Hanson, and E.M. Riseman. Extracting straight lines. *IEEE Trans. on Pattern Analysis and Machine Intelligence*, 8:425–455, 1986.

[7] K. Daniilidis, A. Makadia, and T. Blow. Image processing in catadioptric planes: Spatiotemporal derivatives and optical flow computation. In *Omnivis 2002 : Workshop on Omnidirectional Vision, held with ECCV*, pages 3–10, 2002.

[8] R.O. Duda and P.E. Hart. Use of the hough transform to detect lines and curves in pictures. *CACM*, 15(1):11–15, January 1972.

[9] C. Geyer and K. Daniilidis. Catadioptric projective geometry. *International Journal on Computer Vision*, 45(3):223–243, December 2001.

[10] J. Illingworth and J.V. Kittler. A survey of the hough transform. *Computer Vision, Graphics, Image Processing*, 44(1):87–116, October 1988.

[11] Fiala M. and Basu A. Hough transform for feature detection in panoramic images. *Pattern Recognition Letter*, 23(14):1863–1874, 2002.

[12] S.K. Nayar and S. Baker. Catadioptric image formation. In *Image Understanding Workshop 97*, pages 1431–1437, 1997.

[13] Y. Onoe, N. Yokoya, K. Yamazawa, and H. Takemura. Visual surveillance and monitoring system using an omnidirectional video camera. In *International Conference Pattern Recognition 98, Australia*, pages 588–592, 1998.

[14] P.F. Sturm. A method for 3d reconstruction of piecewise planar objects from single panoramic images. In *Omnivis 2000: Workshop on Omnidirectional Vision, held with CVPR*, pages xx–yy, 2000.

[15] Y. Yagi and S. Kawato. Panoramic scene analysis with conic projection. In *International Conference on Intelligent Robots and Systems 1990*, pages 181–187, 1990.

[16] K. Yamazawa, Y. Yagi, and M. Yachida. Omindirectional imaging with hyperboliodal projection. In *International Conference on Intelligent Robots and Systems 1993*, pages 1029–1034, 1993.

[17] X. Ying and Z. Hu. Catadioptric camera calibration using geometric invariants. In *International Conference Computer Vision 2003*, pages 1351–1358, 2003.

[18] Z. Zhang. Parameter estimation techniques: A tutorial with application to conic fitting. *Image and Vision Computing*, 15:59–76, 1997.